Nano Convergence
a SpringerOpen Journal

RESEARCH Open Access

Nanoscale investigation of surface potential distribution of $Cu_2ZnSn(S,Se)_4$ thin films grown with additional NaF layers

Gee Yeong Kim[1], Juran Kim[1], William Jo[1*], Dae-Ho Son[2], Dae-Hwan Kim[2] and Jin-Kyu Kang[2]

Abstract

CZTS precursors [SLG/Mo (300 nm)/ZnS (460 nm)/SnS (480 nm)/Cu (240 nm)] were deposited by RF/DC sputtering, and then NaF layers (0, 15, and 30 nm) were grown by electron beam evaporation. The precursors were annealed in a furnace with Se metals at 590°C for 20 minutes. The final composition of the CZTSSe thin-films was of Cu/(Zn + Sn) ~ 0.88 and Zn/Sn ~ 1.05, with a metal S/Se ratio estimated at ~0.05. The CZTSSe thin-films have different NaF layer thicknesses in the range from 0 to 30 nm, achieving a ~3% conversion efficiency, and the CZTSSe thin-films contain ~3% of Na. Kelvin probe force microscopy was used to identify the local potential difference that varied according to the thickness of the NaF layer on the CZTSSe thin-films. The potential values at the grain boundaries were observed to increase as the NaF thickness increased. Moreover, the ratio of the positively charged GBs in the CZTSSe thin-films with an NaF layer was higher than that of pure CZTSSe thin-films. A positively charged potential was observed around the grain boundaries of the CZTSSe thin-films, which is a beneficial characteristic that can improve the performance of a device.

Keywords: $Cu_2ZnSn(S,Se)_4$; Na; Grain boundary; Surface potential; Kelvin probe force microscopy

1 Background

$Cu_2ZnSn(S,Se)_4$ (CZTSSe) quaternary compound semiconductors are promising materials with characteristics that are desirable for thin-film solar cells. First of all, CZTSSe consists of Zn and Sn, which are abundant, low-cost materials relative to the In and Ga required for $Cu(In,Ga)Se_2$ (CIGS), and therefore CZTSSe has a composition that is promising for commercialization [1,2]. Second, CZTSSe has a direct band gap between 1.0 and 1.7 eV which can be tuned by adjusting the S and Se composition, with the optimum value for solar cells at 1.4 eV [3]. Third, CZTSSe has a high absorption coefficient of approximately 10^5 cm^{-1}, which is similar to that of CIGS [4], and thus the photo-generated carrier can efficiently be absorbed just a few micrometer. However, CZTSSe thin-film solar cells have a conversion efficiency of 12.6%, which is lower than the 20.8% of CIGS solar cells. Also, there are some limitations in producing CZTSSe thin-film solar cells where, for example, the optimal growth conditions are still not well known. In order to reduce gap in the efficiency with CIGS, there are many issues related to CZTSSe compounds that must be solved.

One issue is the effect that Na has on the material. In previous studies, the introduction of Na to CIGS solar cells enhanced the open-circuit voltage (V_{OC}) and the fill factor (FF) [5]. The Na from the soda lime glass diffused out to the CIGS layer, resulting in an improvement in the crystallinity while prohibiting the inter-diffusion of In and Ga. Furthermore, Na increased the hole concentration of the CIGS absorber layer, and it also enhanced the *p*-type conductivity [6,7]. Rudmann *et al.* reported that Na was located at the grain boundaries (GBs) in polycrystalline CIGS and not in the bulk of single CIS [5,8]. Na incorporates into the In and Ga lattice sites as an acceptor, and the In or Ga atoms on the Cu sites [$(In, Ga)_{Cu}$ defects] were replaced with Na on the Cu sites (Na_{Cu}). Thus, Na can reduce the amount of In-Cu antisites (In_{Cu} donors), enhancing the crystallinity [9-11]. In other studies, Na was observed to enhance the efficiency of the solar cells by changing the electronic properties of the cells, such as the electrical passivation, and by improving the atomic motilities [12]. In addition, the Na

* Correspondence: wmjo@ewha.ac.kr
[1]Department of Physics, Ewha Womans University, Seoul, Korea
Full list of author information is available at the end of the article

Springer

© 2014 Kim et al.; licensee Springer. This is an Open Access article distributed under the terms of the Creative Commons Attribution License (http://creativecommons.org/licenses/by/4.0), which permits unrestricted use, distribution, and reproduction in any medium, provided the original work is properly cited.

removed the defect states in the CIGS thin-films, and therefore many acceptor and donor states, as well as defects, around the GB could be altered.

The GB states in CIGS have an increased concentration of free carriers as a result of the passivation by Na. This results in the occurrence of acceptor-like states or in the elimination of donor-like states at the GBs. The effective electron diffusion length of CIGS can then affect the V_{OC} [12]. Yan *et al.* confirmed that Na segregates across the GBs in CIS thin-films grown on SLG. Kelvin prove force microscopy (KPFM) measurements revealed that the GBs in CIS films exhibited a positively charged potential (~200 meV) [13], but on the other hand, the surface of the CIS thin-films grown on borosilicate glass revealed a small potential value lower than 30 meV. Therefore, Na provides a beneficial effect to CIGS thin-films by forming an electrical potential at the GBs due the segregation of Na across GB. Consequently, the positively charged potential at the GBs due to the Na segregation could repel holes and attract electrons, suppressing recombination [13]. The grain boundaries (GBs) of the CIGS act as a factor that improves the performance of the cells, contrary to single crystal thin-film solar cells where GBs act as defects and recombination centers [14,15].

We have already published how the dominant positively charged GBs and the negatively charged IGs on CZTSSe thin-films assist in the efficient carrier collection and carriers separation near the GBs [16,17]. Also, Sutter-Fella *et al.* reported that Na in CZTSSe thin-films formed liquid Na_2Se_x phases, enhancing the grain growth and thereby improving the electronic properties at an optimal thickness of the NaF layer (10 nm) [6]. They suggested that Na accumulated around the GBs, thus improving the carrier collection in the CZTSSe thin-film solar cells. However, a high amount of Na was not sufficiently incorporated into CZTSSe absorber layer. Details on the effects of Na on the GBs of CZTSSe are still lacking. Thus, in this study we used KPFM to carefully investigate the potential distribution around the GBs with respect to the variation of the NaF layer on CZTSSe thin-films.

2 Method

The metal precursors of the CZTSSe layers were grown via RF/DC sputtering, and the staking order was SLG/Mo/ZnS/SnS/Cu. The thickness of each stacked layer was ~460 nm for ZnS, 480 nm for SnS, and 240 nm for Cu. After the deposition of the precursor, the NaF layer was grown on the precursors via electron-beam evaporation at thicknesses of 0, 15, and 30 nm. The precursors were annealed with Se metals in a furnace at 590°C for 20 minutes. The final composition of the CZTSSe thin-films measured through inductively coupled plasma (ICP) was of Cu/(Zn + Sn) ~ 0.88 and Zn/Sn ~ 1.05 . The metal S/Se ratio was estimated to be ~0.05, and the grain sizes of the CZTSSe thin-films were of 1–2 μm, and that of CZTSSe thin-films with the NaF layers were of 4–5 μm, as measured by field emission scanning electron microscopy (FE-SEM) (JSM-6700F).

The KPFM measurements were performed using commercial atomic force microscopy (AFM) (Nanofocus Inc. South Korea, n-Tracer). A Pt/Ir coated tip was used for to measure the topography and the surface potential. In this paper, we calibrated the tip by using a highly oriented pyrolytic graphite (HOPG) sample. The topographic and KPFM images were obtained under a non-contact mode at a resonant frequency of the probe of about 78.3 kHz. The scanning rate was set to 0.5 Hz to minimize the topological signal. The work function of the HOPG was generally known to be 4.6 eV [18]. The KPFM tool is widely used to characterize semiconductors, such as for obtaining the surface potential

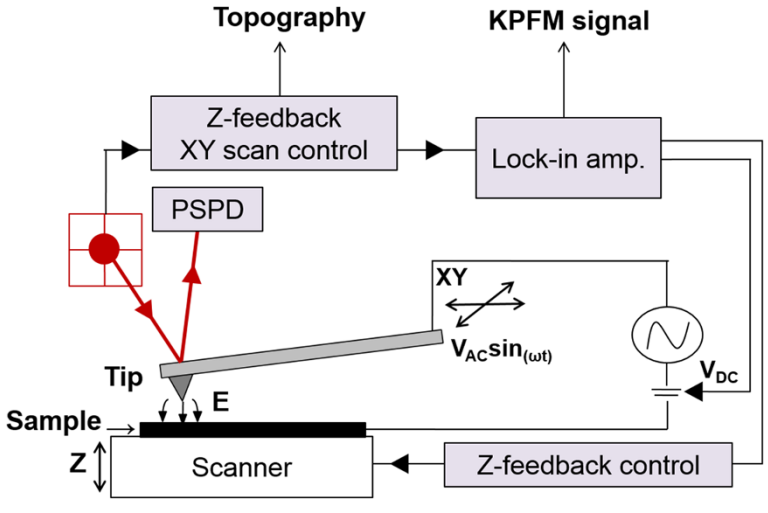

Figure 1 Schematic illustration of Kelvin probe force microscopy and surface potential measurement system.

and the work function of the sample surface at a nanoscale. From the KPFM measurements, we can obtain the contact potential difference (V_{CPD}) (i.e., the surface potential) which is different from using a metallic AFM tip and obtaining the sample work function.

The V_{CPD} can be defined as in Eq. 1. If the tip approaches the sample, then an electrostatic force forms between the metal tip and the surface of the sample. When the tip approach to the sample surface, the Fermi levels of the tip and the sample achieve a state of equilibrium. In the equilibrium state, a V_{CPD} forms as a result of the difference in the vacuum level. An external bias DC voltage (V_{DC}) nullifies the V_{CPD}, forming a feedback system, as shown in Figure 1. The V_{DC} has the same magnitude as the V_{CPD}, and the V_{CPD} has the same values as the work function difference between the tip and the sample. Furthermore, an AC voltage (V_{AC}) can also be applied to the tip at an amplitude of 1 V with a frequency of 70 kHz, together with the V_{DC}, and the V_{AC} enables the oscillation of electrical forces on the tip.

$$V_{CPD} = \frac{\phi_{tip} - \phi_{sample}}{-e} \tag{1}$$

We can consider the metal tip and the surface of the sample to form a capacitor. Thus, the electrostatic force of tip and the sample [F(z)] can be defined as in Eq. 2. The ∂C/∂z is the gradient of the capacitance, and F(z) is the equation where ΔV is the potential difference between V_{CPD} and the voltage applied to the tip. The equation for the electrostatic force applied to the tip can be divided into three terms, as shown in the first term from Eq. 3. The first term is inserted here in Eq. 2, and we can then obtain Eq. 3. Eq. 3 is divided into three parts. In the first part of Eq. 3, F_{DC} (Eq. 4) represents the static deflection of the tip that is used, and F_{ω} (Eq. 5) and $F_{2\omega}$ (Eq. 6) oscillate with frequencies proportional to ω. F_{ω} in Eq. 5 generally measures the V_{CPD}, and $F_{2\omega}$ is used for capacitance microscopy [19].

$$F(z) = -\frac{1}{2}\Delta V^2 \frac{dC(z)}{dz} \tag{2}$$

$$F = F_{DC} + F_{\omega} + F_{2\omega} \tag{3}$$

$$F_{DC} = \frac{dC}{dz}\left[\frac{1}{2}(V_{DC} \pm V_{CPD})^2\right] \tag{4}$$

$$F_{\omega} = -\frac{dC}{dz}(V_{DC} \pm V_{CPD})V_{AC}\sin(\omega t) \tag{5}$$

$$F_{2\omega} = \frac{1}{4}\frac{dC}{dz}V^2{}_{AC}[\cos(2\omega t) - 1] \tag{6}$$

3 Result and discussion

The CZTSSe thin-films deposited by sputtering method have different thicknesses in the NaF layer: 0 (a), 15 (b), and 30 nm (c). The CZTSSe thin-films contain ~4% of Na. The efficiency of the CZTSSe solar cell is almost

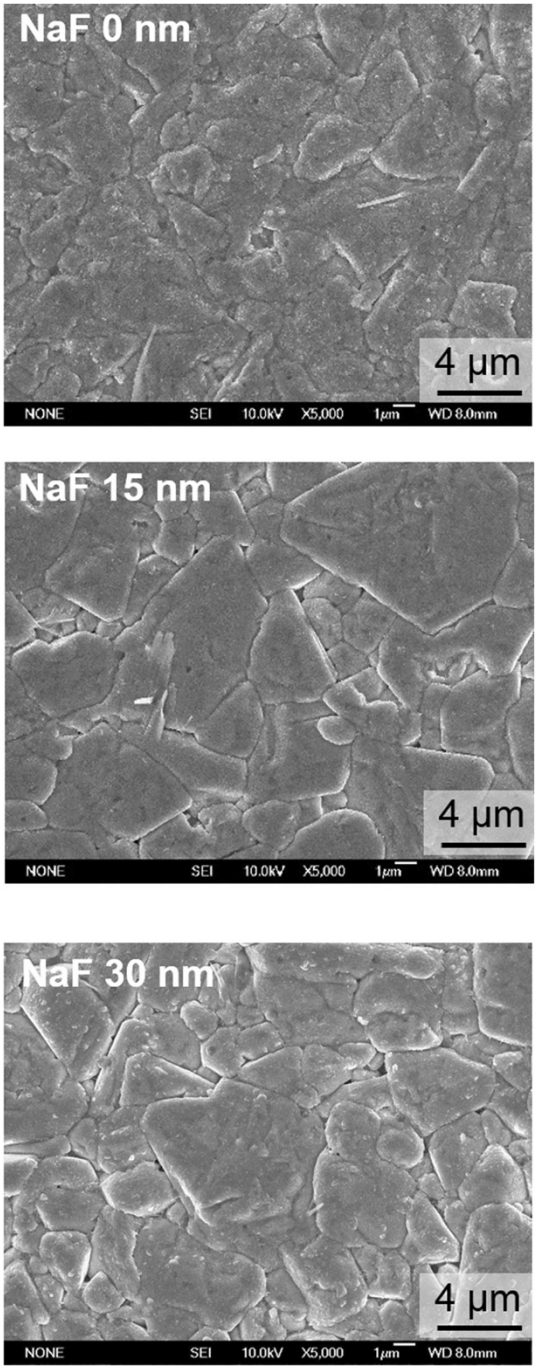

Figure 2 Scanning probe microscopy images of (a) NaF (0 nm)/CZTSSe (b) NaF (15 nm)/CZTSSe (c) NaF (30 nm)/CZTSSe thin-films deposited by sputtering method. The NaF/CZTSSe thin-film surface shows the higher grain size.

similar at ~3%. The grain size of the CZTSSe thin-films increases by adding NaF, as compared to the thin-films without an NaF layer, as shown in Figure 2. The CZTSSe thin-films without NaF presented a grain size of 1–2 μm, and that with an NaF layer was of 4–5 μm. The surface uniformity also improved by adding an NaF layer.

Figure 3 shows the topographic and the surface potential images of the CZTSSe thin-films with and without an NaF layer. The topographic images and the line profile results showed that the height of GBs in the CZTSSe thin-films with the NaF layer were reduced from 400 nm to 100 nm. We also obtained the root mean square (RMS) roughness of the CZTSSe to be 177 nm, and the films with the NaF layer had a lower roughness of 106 nm (15 nm NaF) and 112 nm (30 nm NaF). Thus, adjustments of the NaF layer thickness were observed to influence the grain growth and the formation of a uniform surface. Figures 3(d)–(f) show the surface potential images taken through KPFM measurements. The yellow region represents the positive surface potential values, and the blue region represents the negative potential values. Figures 3(e) and (f) exhibit the images of the potential mapping, and the potential near the GBs with an NaF layer increase relative to that without NaF [Figure 3 (d)]. In the CZTSSe films with NaF, the ratio of the yellow regions, especially that near the GBs, is larger than that of pure CZTSSe thin-films.

Figure 4(a)–(c) presents the line profile of the topographic, and the surface potential images are marked with a red line, as shown in Figure 3. Figures 4(d)–(f) show the total potential distribution of the CZTSSe thin-films with respect to the thickness of the NaF layers. In Figures 4 (a)–(c), the CZTSSe thin-films show that a negative potential value of about −100 mV at the half region of the GBs and a positive potential of about 110 mV at the IGs, as shown in Figure 4(a). However, the potential of the CZTSSe films with the NaF layer showed a fully positively charged potential of about 120 mV (15 nm NaF) and 380 mV (30 nm NaF) at the GB regions and a negatively charged potential of about −200 mV (15, 30 nm NaF) at the IG regions. The potential distribution was found to be related to the downward band bending because the

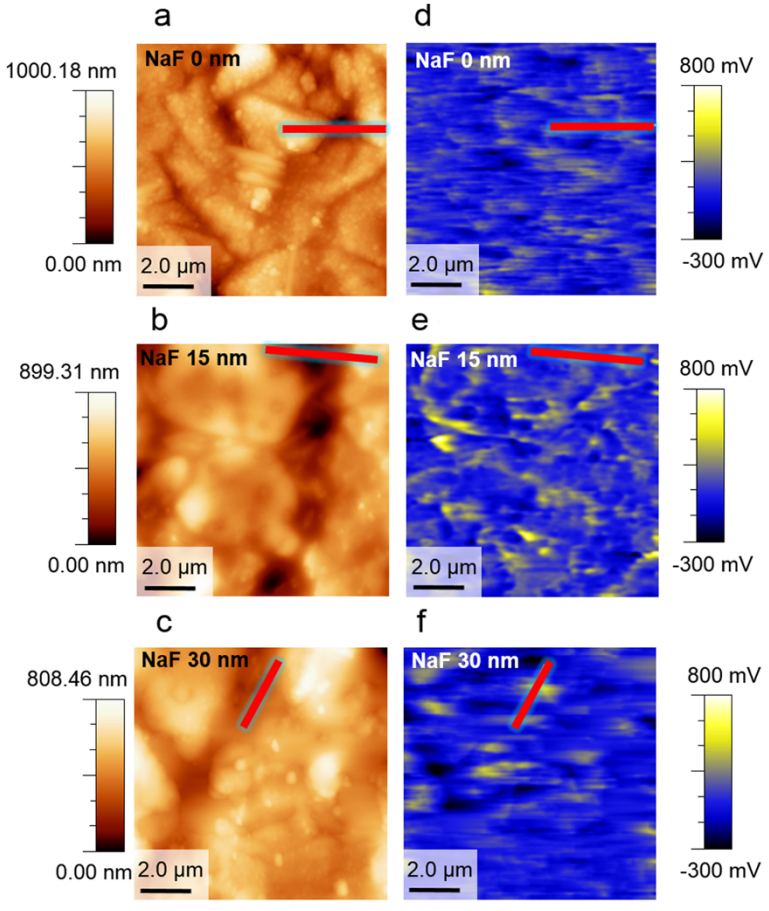

Figure 3 Topography (a) 0 nm (b) 15 nm (c) 30 nm of NaF and surface potential images (d) 0 nm (e) 15 nm (f) 30 nm of NaF of the CZTSSe thin-films. The grain size increase with increasing NaF layer and the potential value is also enhanced.

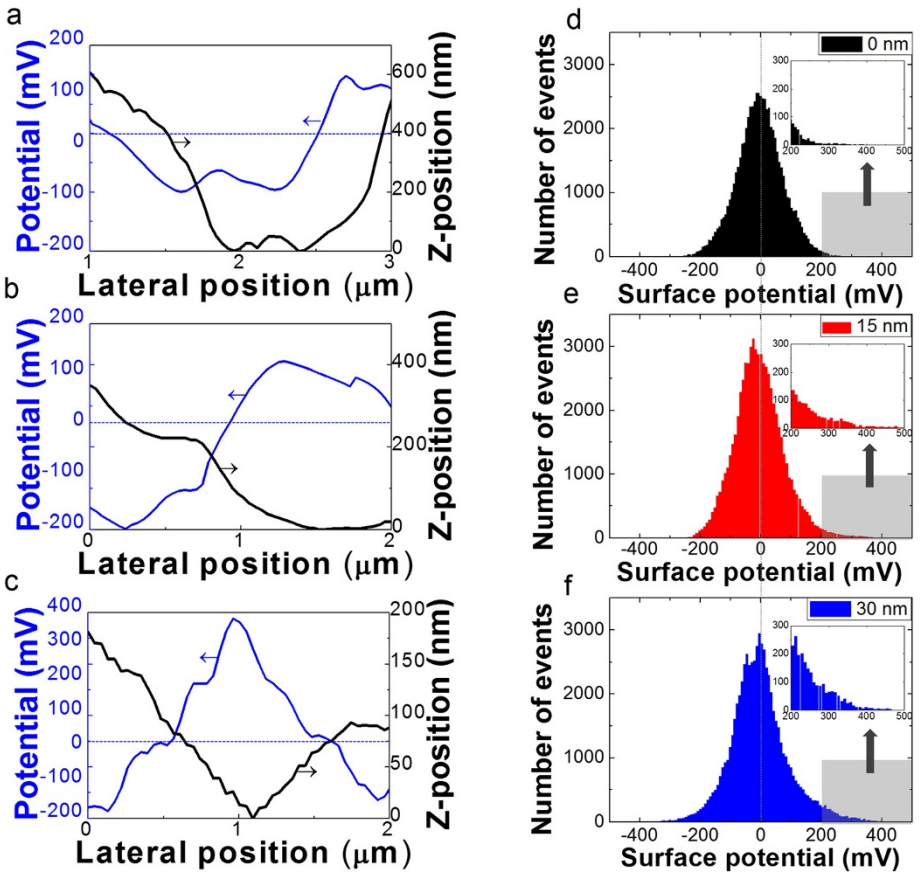

Figure 4 Line profiles of (a) 0 nm (b) 15 nm (c) 30 nm of NaF and potential distribution (d) 0 nm (e) 15 nm (f) 30 nm of NaF with CZTSSe thin-films. Line profiles along the topographic image and the surface potential as indicated red line in Figures 3. The CZTSSe thin-film with NaF shows positively charged potential of the fully GB region.

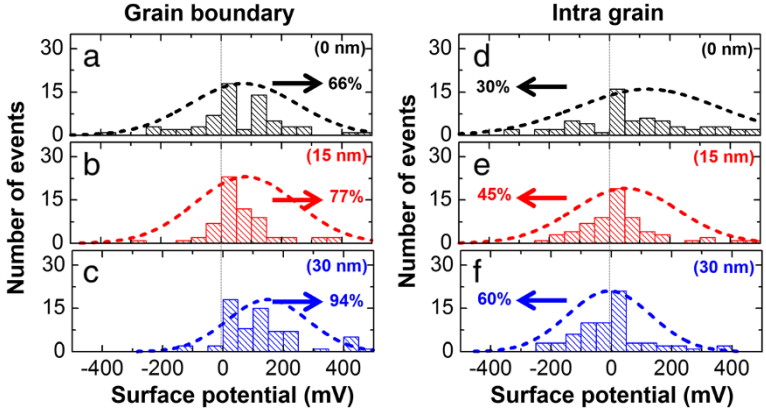

Figure 5 Statistical analysis of potential histogram at the GBs (a) 0 nm (b) 15 nm (c) 30 nm of NaF and IGs (a) 0 nm (b) 15 nm (c) 30 nm of NaF on CZTSSe thin-films. The histogram obtained based on the line profiles results of in regions of near of each sample, respectively. Higher positive potential ratio at GBs and lower negative potential ratio at IGs are exhibited in CZTSSe thin-film with NaF.

positive potential at GBs led to a reduction in the work function near the GBs in CZTSSe.

The positive potential distribution was higher as the NaF layer became thicker for the CZTSSe films, as shown in Figure 4(f). Thus, the potential value was the highest for the 30 nm NaF layer CZTSe film. In previous studies, many groups had reported benign behaviors of the GBs in polycrystalline CIGS thin-film solar cells

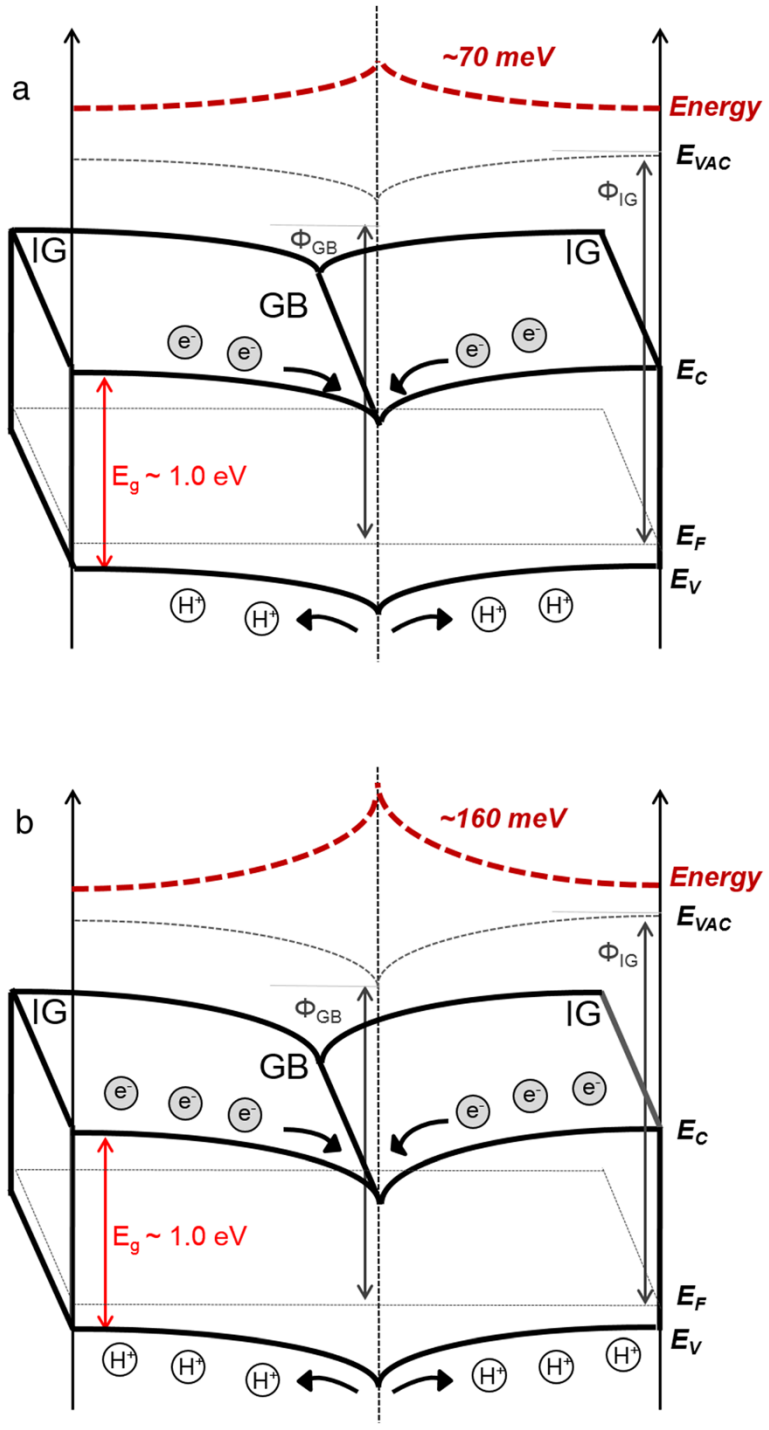

Figure 6 The schematics of band diagram around GB in (a) without NaF and (b) with NaF layer in CZTSSe thin-films. The surface potential energy increases 160 meV around grain boundary with NaF layer. In case **(b)** Electron–hole carriers more efficiently help separate at the GB.

[20]. Jiang *et al.* confirmed the presence of a positively charged potential (smaller work function) at the GBs, as compared to that at the IGs, with a formation of a local built-in potential near the GBs. This can explain how electrons are drawn to the GBs and how holes are repelled from the GB. This is beneficial for carrier collection, and it also suppresses recombination at the GBs. Therefore, the local built-in potential on GBs in the CIGS thin-films plays a critical role to achieve the desired device performance and efficiency [14,15].

Meanwhile, the GBs of the CZTSSe thin-films exhibit similar electrical properties to those of GBs in CIGS thin-films. A higher positive surface potential was measured at the GBs relative to that measured at the IGs, and a current flowed through the GBs of CZTSSe thin-films. This could improve the minority carrier collection near the GBs, and thus, the GBs are one of the essential factors that can enhance the high conversion efficiency of CZTSSe thin-film solar cells [21].

Furthermore, our group reported the presence of the positive potential ratio at the GBs and a negative potential ratio at the IGs in CZTSSe thin-film, and these are closely related to device properties, especially to the J_{SC}. The high conversion efficiency of the GBs of the CZTSSe thin-film consists of dominant, positively charged GBs and negatively charged IGs. This leads to a downward band bending at the GBs and an upward band bending at the IGs, which helps in carrier collection and suppresses the recombination at GBs that are limited to downward band-bended GBs. Thus, the J_{SC} and the shunt resistance are enhanced [16], and therefore we tried to characterize the effects of the GB on the CZTSSe film with respect to the presence of an NaF layer.

Figure 5 shows a histogram from the statistical analysis of the potential value, focusing on the GBs and the IGs in the CZTSSe with and without NaF. The results are based on the line profiles of the regions of near GBs, and the histograms exhibit a positive potential distribution at the GBs as shown in Figures 5(a)–(c) and a negative potential distribution ratio at the IGs as shown in Figures 5(d)–(f). The CZTSSe samples exhibit a lower positive potential ratio of 66% at the GBs and also a lower negative potential ratio of 30% at the IGs. However, the CZTSSe with NaF indicates a higher positive potential ratio of 77% (15 nm of NaF) and 94% (30 nm of NaF) at the GBs and a negative potential ratio of 45% (15 nm of NaF) and 60% (30 nm of NaF) at the IGs. The average potential at the GBs in the CZTSSe thin-film is of 74 mV, and that of CZTSSe with a 15 nm NaF thin-film is of 93 mV. The highest average potential of about ~160 mV is shown in the 30 nm NaF thin-films. Therefore, we conclude that the average potential at the GBs increases by adding NaF.

Figure 6(a) displays the schematics of a band diagram near the GBs in the CZTSSe thin-films, and Figure 6(b) shows the CZTSSe thin-films with a 30 nm NaF layer. The higher thickness of the NaF layer enhances the positively charged (i.e. lower work function) GBs in the CZTSSe layer. In previous studies, the Na on the surface was observed to cause surface dipoles, and thus the dipoles may increase the potential near the GBs in the CIGS surface due to the higher Na concentration around the GBs than around the IGs [13]. Thus, Na could enhance the positively charged GBs in the CIGS thin-film surface, which is a phenomenon consistent with our results. The potential at the GB increases by almost 100 meV with the NaF layer in the CZTSSe absorber, as shown in Figure 6 (b). Moreover, the ratio of the positively charged potential at the GBs and the negatively charged potential at the IG increased with the NaF layer in the CZTSSe thin-films. The electronic properties of the material should be able to efficiently collect the electrons and the holes, helping in the separation around GBs where an NaF layer was added to the CZTSSe. However, it is essential to understand the defect states and the Na passivation through the GBs in CZTSSe layer in order to identify the influence of Na in the CZTSSe solar cells.

4 Conclusion

We investigated the surface potential of CZTSSe thin-films with different thicknesses of the NaF layer by KPFM measurement. The potential value at the GBs relatively increased from 74 mV to 160 mV as the NaF thickness increased. In addition, the ratio of the positively charged GBs and that of the negatively charged IGs in CZTSSe thin-films also increased as the NaF layer increased. In these studies, the Na in CZTSSe layer was observed to have an electronically benign behaviors, efficiently collecting carriers and suppressing the recombination near the GBs.

Abbreviations

CIGS: $Cu(In,Ga)Se_2$; CZTSSe: $Cu_2(Zn,Sn)(S,Se)_4$; GBs: Grain boundaries; IGs: Intragrains; KPFM: Kelvin probe force microscopy; V_{oc}: Open-circuit voltage; J_{sc}: Short-circuit current; F.F.: Fill factor; Eff.: Photo-conversion efficiency.

Competing interests

The authors declare that they have no competing interests.

Authors' contributions

GYK, JRK, and WJ measured the electrical properties of the CZTSSe samples using scanning probe microscopy. DHS, DHK, and JKK fabricated the CZTSSe samples by sputtering with subsequent selenization. All authors read and approved the final manuscript.

Acknowledgements

This work was supported by the New & Renewable Energy of the Korea Institute of Energy Technology Evaluation and Planning (KETEP), grant funded by the Korea government, Ministry of Trade, Industry and Energy (No. 20123010010130).

Author details

[1]Department of Physics, Ewha Womans University, Seoul, Korea. [2]Daegu Gyeongbuk Institute of Science and Technology (DGIST), Daegu, Korea.

Received: 12 August 2014 Accepted: 20 August 2014
Published online: 08 October 2014

References

1. S Chen, XG Gong, A Walsh, S-H Wei, Electronic structure and stability of quaternary chalcogenide semiconductors derived from cation cross-substitution of II-VI and I-III-VI_2 compounds. Phys. Rev. B **79**, 165211 (2009)
2. TK Todorov, J Tang, S Bag, O Gunawan, T Gokmen, Y Zhu, DB Mitzi, Beyond 11% efficiency: characteristics of state-of-the-Art Cu2ZnSn(S, Se)4 solar cells. Adv. Energy Mater. **3**, 34–38 (2013)
3. JJ Scragg, J Phillip, LM Peter, Towards sustainable materials for solar energy conversion: preparation and photoelectrochemical characterization of Cu_2ZnSnS_4. Electrochem. Commun. **10**, 639–642 (2008)
4. AR Jeong, W Jo, DY Park, H Cheong, YK Seo, JH Park, JS Chung, YS Lee, Y-J Kwark, Effect of substrates on structural and optical properties of Cu-poor $CuGaSe_2$ thin films prepared by in-situ co-evaporation. Curr. Appl. Phys. **13**, 907–912 (2013)
5. D Rudmann, AF da Cunha, M Kaelin, F Kurdesau, H Zogg, AN Tiwari, G Bilger, Efficiency enhancement of Cu(In, Ga)Se2 solar cells due to post-deposition Na incorporation. Appl. Phys. Lett. **84**, 1129 (2004)
6. CM Sutter-Fella, JA Stückelberger, H Hagendorfer, FL Mattina, L Kranz, S Nishiwaki, AR Uhl, YE Romanyuk, AN Tiwari, Na assisted sintering of chalcogenides and its application to solution processed Cu2ZnSn(S, Se)4 thin film solar cells. Chem. Mater. **26**, 1420–1425 (2014)
7. T Nakada, D Iga, H Ohbo, A Kunioka, Effects of Na on Cu(in, Ga)Se2-based thin films and solar cells. Jpn. J. Appl. Phys. **36**, 732–737 (1998)
8. MA Contreras, B Egaas, D King, A Swartzlander, T Dullweber, Texture manipulation of $CuInSe_2$ thin film. Thin Solid Films **361–362**, 167–171 (2000)
9. MA Contreras, B Egaas, P Dippo, J Webb, J Granata, K Ramanathan, S Asher, A Swartzlander, R Noufi, On the role of Na and modifications to CIGS absorber materials using thin MF (M=Na, K, Cs) precursor layers. Conference Record of the Twenty Sixth IEEE Photovoltaic Specialists Conference 359–362 (1997). DOI 10.1109/PVSC.1997.654102.
10. BJ Stanbery, C-H Chang, TJ Anderson, Engineered phase inhomogeneity for CIS device optimization. Proc of the 11th Int Conf on Ternary and Multinary Compounds **152**, 915–922 (1998)
11. BJ Stanbery, S Kincal, S Kim, TJ Anderson, OD Crisalle, SP Ahrenkiel, G Lippold, Role of Na in the control of defect structures in CIS. Conference Record of the Twenty Eighth IEEE Photovoltaic Specialists Conference 440–445 (2000). DOI 10.1109/PVSC.2000.915864.
12. A Rockett, The electronic effects of point defects in $Cu(In_xGa_{1-x})Se_2$. Thin Solid Films **361–362**, 330–337 (2000)
13. Y Yan, C-S Jiang, R Noufi, S-H Wei, HR Moutinho, MM Al-Jassim, Electrically benign behavior of grain boundaries in polycrystalline $CuInSe_2$ films. Phys. Rev. Lett. **99**, 235504 (2007)
14. C-S Jiang, R Noufi, JA AbuShama, K Ramanathan, HR Moutinho, J Pankow, MM Al-Jassim, Local built-in potential on grain boundary of Cu(In, Ga)Se2 thin film. Appl. Phys. Lett. **84**, 3477–3479 (2004)
15. C-S Jiang, R Noufi, K Ramanathan, JA AbuShama, HR Moutinho, MM Al-Jassim, Does the local built-in potential on grain boundaries of Cu(In, Ga) Se2 thin films benefit photovoltaic performance of the device? Appl. Phys. Lett. **85**, 2625–2627 (2004)
16. GY Kim, AR Jeong, JR Kim, W Jo, D-H Son, D-H Kim, J-K Kang, Surface potential on grain boundaries and intragrains of highly efficient Cu2ZnSn(S, Se)4 thin-films grown by two-step sputtering process. Sol. Energy Mater. Sol. Cells. **127**, 129–135 (2014)
17. GY Kim, JR Kim, W Jo, D-H Son, D-H Kim, J-K Kang, Nanoscale observation of surface potential and carrier transport in Cu2ZnSn(S, Se)4 thin films grown by sputtering-based two-step process. Nanoscale Res. Lett. **9**, 10 (2014)
18. W Melitz, J Shen, S Lee, JS Lee, AC Kummel, R Droopad, ET Yu, Scanning tunneling spectroscopy and Kelvin probe force microscopy investigation of Fermi energy level pinning mechanism on InAs and InGaAs clean surfaces. J. Appl. Phys. **108**, 023711 (2010)
19. W Melitz, J Shen, AC Kummel, S Lee, Kelvin probe force microscopy and its application. Surface Science report **66**, 1–27 (2011)
20. RH Shin, AR Jeong, W Jo, Investigation of local electronic transport and surface potential distribution of Cu(In, Ga)Se2 thin-film. Curr. Appl. Phys. **12**, 1313–1318 (2012)
21. JB Li, V Chawla, BM Clemens, Investigating the role of grain boundaries in CZTS and CZTSSe thin film solar cells with scanning probe microscopy. Adv. Mater. **24**, 720–723 (2012)

doi:10.1186/s40580-014-0027-1
Cite this article as: Kim *et al.*: **Nanoscale investigation of surface potential distribution of $Cu_2ZnSn(S,Se)_4$ thin films grown with additional NaF layers.** *Nano Convergence* 2014 **1**:27.

Submit your manuscript to a SpringerOpen journal and benefit from:

► Convenient online submission
► Rigorous peer review
► Immediate publication on acceptance
► Open access: articles freely available online
► High visibility within the field
► Retaining the copyright to your article

Submit your next manuscript at ► springeropen.com